Solvent effect on the ion adsorption from ionic liquid electrolyte into sub-nanometer carbon pores

R. Lin[a,1], P. Huang[a], J. Ségalini[a], C. Largeot[a], P.L. Taberna[a], J. Chmiola[b,2,3], Y. Gogotsi[b,3], P. Simon[a,*,3]

[a] Université de Toulouse, CIRIMAT, UMR-CNRS 5085, 31062 Toulouse Cedex 4, France
[b] Department of Materials Science and Engineering and A.J. Drexel Nanotechnology Institute, Drexel University, Philadelphia, PA 19104, USA

A B S T R A C T

This paper presents the results from the investigation of the influence of ion size on the capacitance behaviour of TiC-derived carbon (CDC) powders in the ethyl-methylimmidazolium-bis(trifluoromethane-sulfonyl)imide ionic liquid (EMI, TFSI) used as neat electrolyte at 60 °C or as salt dissolved in acetonitrile and tested at room temperature. These studies were carried out with the assembly of conventional 3-electrode electrochemical cells as well as using the Cavity-MicroElectrode (CME) technique. The issues regarding the extents of desolvation of the electrolyte ions when adsorbed in the pores of the CDCs under applied potential were studied, the CME technique was found to be particularly efficient in the deduction of the effective ion size under solvated conditions.

Keywords:
Double layer capacitors
Carbon
Sub-nanometer pore
Adsorption
Solvation effect
Extra-capacitance

1. Introduction

The development of supercapacitors in the field of energy storage and conversion is of increasing importance to provide high power for different system requirements [1,2]. Electrochemical double layer capacitors (EDLCs) are a class of electrochemical capacitors (ECs) that store the charge electrostatically through reversible adsorption of ions from an electrolyte onto a high surface area carbon. Hence, electrochemical double layer charge/discharge knowledge and understanding are the required fundamentals encompassing supercapacitor technology in light to improve on interfacial and electrochemical aspects.

In order to obtain reversible high charge storage and high power capability of EDLCs, high specific surface area carbons are required [3]. However, the ion-adsorption mechanism not only involves the carbons but also the electrolyte ions that make up the electric double layer. The traditional understanding of how the porosity affects specific capacitance and frequency response initially holds that pores larger (at least twice) than the size of the electrolyte bare ion plus its solvation shell are required for maximizing specific capacitance of the carbon. Several authors raised issue on the extent of solvation shell of the ions entering into pores and emphasized the importance of correlation between pore size and EDL capacitance [4–12]. Finally, this basic assumption of the needs for pore sizes to be about twice the solvated ions was then shown to be more complex and maximum capacitance was shown to be achieved with micropores leading to an increase in capacitance in sub-nanometer pores [13]. It was explained by partial desolvation of the electrolyte ions in pores smaller than the solvated ion size. These results were obtained using titanium carbide-derived carbons (Ti-CDCs) as model materials which enable systematic study of pore size effects thanks to their uni-modal pore size distribution, where the pore size control is achieved by varying synthesis parameters [13]. Following this work, many studies confirmed these results since maximum capacitance at the respective positive and the negative electrode for anion and cation adsorption, respectively, was obtained at pore size smaller than the solvated ion size and a model explaining this effect was developed [14–16]. Aurbach's group [17] also recently demonstrated that sub-nanometer pores were accessible to ions, thus confirming all the recent results on capacitance of carbon with sub-nanometer pores obtained during the last couple of years. Further study carried out in a two-electrode cell using ionic liquid as a solvent-free electrolyte showed that the maximum cell capacitance was achieved when ion size was in proximity of pore size [18]. This maximum cell capacitance was achieved when sizes of pores match those of the

* Corresponding author.
E-mail address: simon@chimie.ups-tlse.fr (P. Simon).
[1] Solvionic, Site SNPE, Chemin de la Loge, 31078 Toulouse cedex 4, France.
[2] Lawrence Berkeley National Laboratory, Environmental Energy Technologies Division, 1 Cyclotron Road, Berkeley, CA 94720, USA.
[3] ECS Active Member.

adsorbing ions of the electrolyte raised some important questions regarding the double layer charging in pores smaller than 1 nm.

The aim of this paper is to go further into the understanding of the relationship between the ion size, its solvation shell, and the pore size, as a continuation of our initial work done using a 2-electrode cell and published as a short communication [18] and also, to address the issue previously raised by several authors [4,5,8,19] on the importance of understanding solvation/desolvation effects. We extended the experiments on Ti-CDCs in neat 1-ethyl-3-methyl-imidazolium bis(trifluoro-methane-sulfonyl)-imide (EMI, TFSI) ionic liquids using a three-electrode cell configuration, allowing the discrimination between the cation and the anion capacitive behaviour. Then, we will show the influence of the ionic solvation by carrying out the electrochemical characterizations of the CDCs in 2 M solution of EMI, TFSI dissolved in acetonitrile as an electrolyte. The comparison between these two sets of experiments should lead to a better understanding of the ion size and the solvation effect onto the ion adsorption in porous carbons.

2. Experimental

EMI, TFSI ionic liquid was obtained from Solvionic and extra-dry acetonitrile (AN) (CAS 75-05-8) was purchased from Acros Organics.

Ti-CDC samples were prepared by chlorinating TiC powders (Alfa Aesar #40178, particle size 2 μm) in a flow of chlorine at 400, 500, 550, 600, 700, 800, 900 and 1000 °C for 3 h in a horizontal quartz tube furnace followed by annealing at 600 °C for 2 h to ensure the removal of metal chlorides and unreacted chlorine. Maximum elimination of atmospheric gas and atoms adsorbed on the walls of reaction tube and carbide surfaces was ascertained by passing Argon (99,998%) through the reaction tube during heating and cooling of the furnace.

Argon sorption was conducted from relative pressure P/P_0 of 10^{-6} to 1 to assess porosity and surface area data. Porosity analysis was carried out with Ar and N_2 at liquid nitrogen temperature, −195.8 °C, and with CO_2 at 0 °C, on samples outgassed for at least 12 h at 300 °C using a Quantachrome Autosorb-1. Isotherms show increasing pore volume with increasing synthesis temperature. All isotherms are type I suggesting that CDC is microporous according to the IUPAC classification (not shown, see ref. [13] for details). At 1000 °C chlorination temperature, there is a slight hysteresis showing a small amount of mesoporosity. Pore size distributions reported were calculated from Ar adsorption data using the nonlocal density functional theory (NLDFT) method [20] for slit shaped pores provided by Quantachrome data reduction software version 1.2 and the SSA was calculated using the Brunauer, Emmet, Teller (BET) [21]. N_2 sorption was used to ensure that samples did not have large mesopores, not shown by Ar sorption, and CO_2 sorption was done to ensure that there is no significant volume of micropores, that is not accessible by Ar. Since the difference between Ar, N_2 and CO_2 pore volumes was minimal, only the Ar results were used in this article.

Structure and properties of Ti-CDC have been described in detail in our previous publications [13,14,21] as well as pore size and porous volume [18] and will not be discussed here. The 900 °C sample newly prepared for this work has a mean pore size of 1.0 nm and a porous volume of 0.8 $cm^3\ g^{-1}$ in the same conditions. The mean pore size value corresponds to 85% of pore volume below this size Values were measured on the same batch of CDC that was used for electrochemical measurements in this work. This provides the highest accuracy and eliminates possibility that some uncontrolled deviations in the synthesis process may affect the electrochemical data.

Two different experimental set-ups were used to carry out the electrochemical investigation.

Electrode films for the standard 4 cm^2 supercapacitor cell were prepared by mixing 95 wt% CDC with 5 wt% PTFE. The thickness of the active material ranged from 250 to 270 μm depending on the synthesis temperatures of the Ti-CDCs, while keeping the weight density constant at 15 mg/cm^2. Large area supercapacitor cells were assembled in a glove box with an Argon atmosphere of less than 1 ppm of O_2 and H_2O content. The active materials were laminated onto treated aluminium current collectors [22,23] and the stack was completed with a polytetrafluoroethylene separator (2 × 25 μm) inserted between the two electrodes. A constant pressure of about 5.10^5 Pa was applied to the stack with the help of PTFE slabs and stainless steel clamps. All cells tested were assembled symmetrically. Silver wire (2 mm in diameter) was used as a quasi-reference electrode with the assumption that the concentration at the silver electrode did not change during cycling, hence keeping its potential constant. The cell was then immersed in neat EMI, TFSI and tested at 60 °C. Galvanostatic cycling tests were carried out at current density of 5 mA/cm^2 applied on the cells. All electrochemical measurements were made using a multichannel VMP3 Potentiostat/galvanostat (Biologic Science Instruments).

Specific capacitance, C, in Farad per gram of CDC per electrode (F/g) was calculated from the slope of the galvanostatic discharge plot, dV/dt ($V\ s^{-1}$), of the 10th galvanostatic cycle by (Eq. (1)):

$$C = \frac{nI}{(dV/dt) \times m} \quad (1)$$

where n takes the number of 1 or 2 depending on determining individual electrode (1) or cell (2) capacitance respectively, I is the current (A), and m the mass of the working electrode (g).

The Cavity Micro-Electrode (*CME*) technique [24] was used to study the effect of solvation of 2 M EMI, TFSI in excess electrolyte of acetonitrile. Such an electrode allows the characterizations of a small amount of powder (hundreds of μg, depending of the size of the cavity) at high scan rates [25]. As compared with conventional electrodes, the real electrochemical interface area is around a fraction of mm^2 and the ohmic drop arising from the bulk of the electrolyte can be neglected, allowing the use of scan rates of few V/s [24,26] to characterize the powder electrode. Details of the CME fabrication and experimental set-up have been previously reported [19,26]. The cavity volume was 10^{-3} mm^3. Four samples of Ti-CDCs synthesized at 500, 600, 800 and 900 °C were used for this investigation. The microcavity of the CME was packed with the various CDC samples by pressing it against the carbon powders in a Petri dish. Cleaning of the cavity was achieved in an ultrasonic bath in an alcohol solution between two experiments. The counter electrode was a rolled platinum foil of 1 cm^2 with a silver rod (2 mm in diameter) as a quasi reference electrode. All obtained results were fully reproducible. The CME tests were performed at room temperature in 2 M EMI, TFSI in AN using a 3-electrode cell configuration.

The solvated ion size was calculated using HyperChem software on 24 nm × 24 nm × 24 nm cells with solute ions (EMI^+ and/or $TFSI^-$) surrounded by 160 molecules of AN. After an optimization of the geometry, a Molecular Dynamics (MD) simulation was run for 2 ps with 0.1 fs intervals. The position was recorded every 1 fs and the radial distribution function (RDF) was then averaged for the 1001 steps.

3. Results and discussion

3.1. Electrochemical behaviour of neat EMI, TFSI in 3-electrode cells

All cyclic voltammetry (CV) and galvanostatic cycling (GC) plots for all CDC samples show a typical capacitive behaviour characterized by a rectangular shape and linear charge/discharge

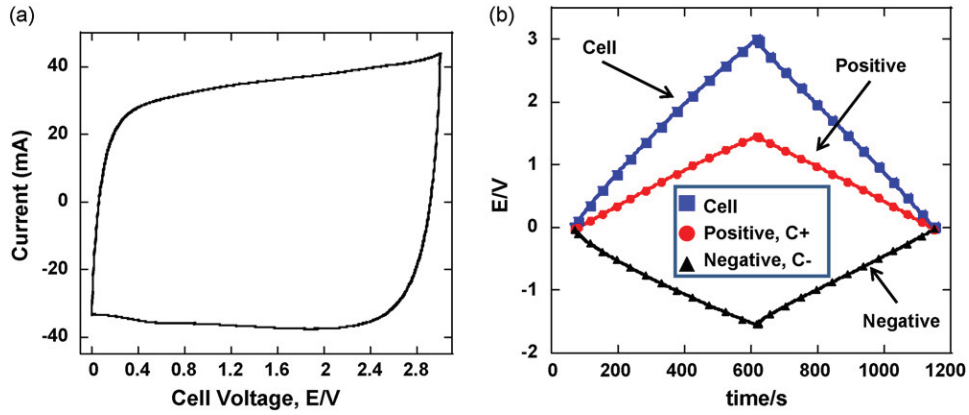

Fig. 1. CV (a) and galvanostatic cycling (GC) (b) of the 900 °C CDC sample with pore size 1.0 nm in neat EMI, TFSI electrolyte.

profiles as can be seen in Fig. 1. These results ensure that the values collected were purely due to adsorption of the electrolyte ions onto the carbon surface, i.e. without any faradaic reactions. In all these experiments, the cell potential was controlled between 0 and 3 V while at the same time each individual electrodes, capacitance values were recorded. Specific capacitance of the cell, as well as for the positive and negative electrodes obtained for the different CDC samples in neat EMI, TFSI electrolyte at 60 °C are presented in Fig. 2a (F/g versus pore size) and b (normalized capacitance in F cm^{-2} versus pore size).

The cell capacitance values of all the cells tested in EMI, TFSI were found to be comparable with the data from a 2-electrode cell [18]. New data points for additional pore sizes added to this plot did not change the trend. As mentioned previously, capacitances of both positive and negative electrodes were measured while controlling the cell voltage to gain an understanding of capacitance contributions from the individual electrodes. Results obtained show a maximum cell capacitance value of 160 F/g at a pore size of 0.72 nm. In terms of the individual electrode capacitance, the anionic adsorption shows a maximum value of capacitance 165 F/g at 0.72 nm, while for the cationic adsorption a peak capacitance value of 153 F/g was observed at the same pore size. Both ions can be considered as spheres whose effective diameter takes into account the longest dimension of the ion, i.e. 0.76 and 0.79 nm for EMI^+ and $TFSI^-$, respectively. Accordingly, both the anion and cation have the same capacitance, which reached the maximum at the size close to that of the ion size.

However, this Figure does not take into consideration the change of the total surface area that is at the origin of the porous volume. Accordingly, we also normalized capacitance values of the cell, the positive and the negative electrodes by dividing the gravimetric capacitance by the BET specific surface area and then plotted them against the pore sizes of the CDCs (Fig. 2b) allowing capacitance comparison irrespective to the carbon surface area, which varies with the synthesis temperature [21]. Direct convergence of the three maxima appears at a pore size of 0.72 nm, confirming that, for neat EMI, TFSI in the absence of any solvation shell, matching pore size to the ion size yields the highest capacitance. We want to emphasize that for direct comparison to be made with specific surface areas reported for other supercapacitor carbons, BET SSA was used. This method being inaccurate with very small pore sizes, NLDFT SSA was also used, assuming slit pore shape. Normalizing the gravimetric specific capacitance by the NLDFT SSA resulted in the same trend with a maximum of the specific capacitance at 0.72 nm pore size (not shown). The decrease in the normalized capacitance observed for the 1.1 nm pore size sample (1000 °C sample) is suspected to be due to the change from a disordered, amorphous carbon structure to a more organized one like previously mentioned [13].

The results presented here suggest that the concepts of conventional electric double layer theory cannot be applied to ionic liquid ions in sub-nanometer pores. We shift from the traditional pattern of ions adsorbed on each pore wall to the concept of just one ion within the pore diameter. This is in agreement with the Electric

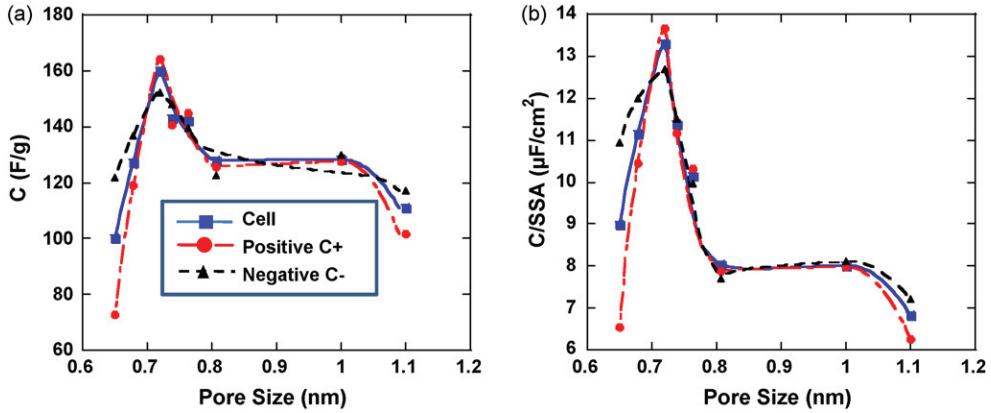

Fig. 2. Capacitance (F/g) versus pore size (a) and normalized capacitance (μF/cm^2) versus pore size (b) plots for the cell, positive and negative electrodes in neat EMI, TFSI electrolyte.

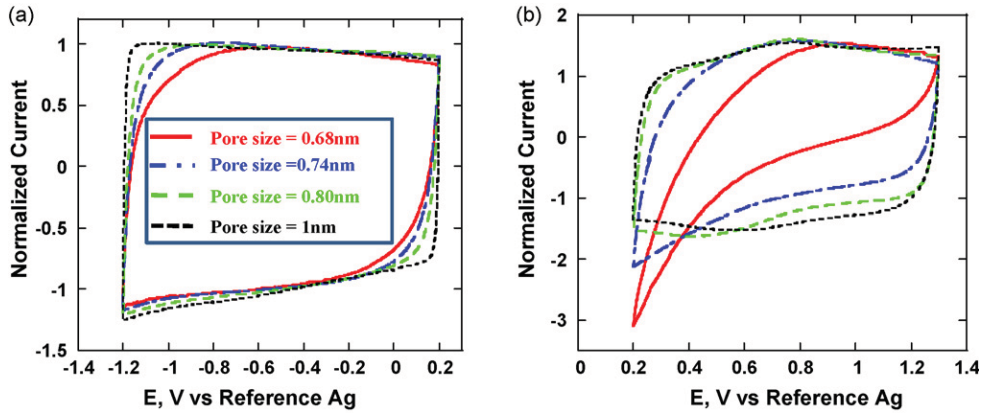

Fig. 3. Normalized CVs of CDC samples in AN + 2 M EMITFSI electrolyte between OCV and −1.2 V/Ref at a scan rate of 100 mV/s (a) and between OCV and +1.3 V/Ref of the CDC samples (b).

Wire-in-Cylinder Capacitor model described by Huang et al. [16,27], where the ions line up along the pore axis.

3.2. Electrochemical behaviour of solvated EMI, TFSI studied using cavity micro-electrodes at 100 mV s^{-1}

CDC samples of pore sizes 0.68, 0.74, 0.8 and 1.0 nm synthesized at 500, 600, 800 and 900 °C, respectively, were used to study the effective ion size of the EMI^+ and $TFSI^-$ ions in AN, when adsorbed in pores of a carbon electrodes. In the same way as in a previous study [19], all CVs have been normalized in current in the pure capacitive behaviour region (at −0.4 V/Ref in Fig. 3a and 1.0 V/Ref in Fig. 3b). This normalization was necessary because the raw CVs measured were of different current response owing to the (i) varying weight of the powder in the CME for each run of experiment and (ii) the difference in the gravimetric capacitance of the respective samples. By doing this, we normalized the linear region of all the electrode CVs to the same capacitance; the shape of the CVs is preserved but comparisons become easier.

The symmetry of CVs gives insights into the ion size/pore size relation as well as the carbon/electrolyte interaction. With such CME, symmetrical distortions of the CVs arise from the resistance in the bulk of the electrolyte in terms of conductivity, that is, the intrinsic property of the electrolyte as a whole. On the other hand, ion accessibility to the carbon porous network, i.e. the ion migration into the pores, could be deduced from asymmetrical current response in the CVs.

3.2.1. EMI^+ adsorption

Fig. 3a shows the normalized CVs of the samples from OCV (measured at about 0.2 V/Ref) to −1.2 V/Ref. During charging from the OCV to −1.2 V/Ref, the EMI^+ ions are adsorbed into the CDC pores and are desorbed when discharging from −1.2 V/Ref to OCV. The CVs of the samples give information on the capacitive behaviour of the carbon/electrolyte couple owing to the interaction between electrolyte ions and the surface of the carbon pores. Here, the CVs of the samples displayed similar capacitive behaviour except for the lowest pore size carbon powder at 0.68 nm where a slight asymmetry of the CV profile upon discharging (from −1.2 up to 0.2 V/Ref) can be observed as compared to charge (from 0.2 down to −1.2 V/Ref). The CVs of the other samples of larger pore sizes (0.74–1 nm) exhibit little deviation from the pure capacitive CV profile, meaning that for these larger pore size CDCs, the carbon pore accessibility is not limited for the EMI^+ ions and accordingly they are able to be adsorbed into the pores of these samples without constraints. Thus, the effective size of the EMI^+ ions when adsorbed in carbon pores can be estimated to be close to 0.7 nm.

3.2.2. $TFSI^-$ adsorption

Fig. 3b shows the CVs of the different CDCs samples recorded in the OCV (i.e. 0.2 V/Ref)–1.3 V/Ref potential range. In this potential window, above the OCV, only anions are involved in the current response during the charging/discharging processes. Anions are adsorbed into the pores of the carbon powders during the positive scans from 0.2 up to +1.3 V/Ref; upon discharging from +1.3 V/Ref down to the OCV value, $TFSI^-$ ions vacate from the pores. CVs collected from CDC samples of pore sizes 0.68 and 0.74 nm are severely distorted asymmetrically while the greater pore size samples (0.8 and 1.0 nm) show near pure capacitive behaviour. These results clearly show that the effective $TFSI^-$ size seen by the carbon during the adsorption process is larger than 0.75 nm.

Fig. 4 shows the CVs collected at a scan rate of 100 mV/s over the entire potential range. Two different potential ranges can be easily distinguished on Fig. 4, above and below the OCV that was measured at 0.2 V/Ref. For the large pore size samples (0.80 and 1 nm pore size), the CVs exhibit the traditional rectangular shape characteristics of a pure capacitive behaviour for both the anion (E > OCV) and the cation (E < OCV), meaning that the effective ion size was smaller than 0.8 nm for both. This confirms the previous results obtained in Fig. 3a and b. For the small pore size samples, the distortions in the CV observed at high potential confirms that the effective size of the $TFSI^-$ ion is larger than ∼0.75 nm, like previously observed. In the low potential range (−0.5 to −1 V/ref), where the cation adsorption occurs, the slight distortion of the CV for the smallest pore size sample (0.68 nm) suggests that the effective EMI^+

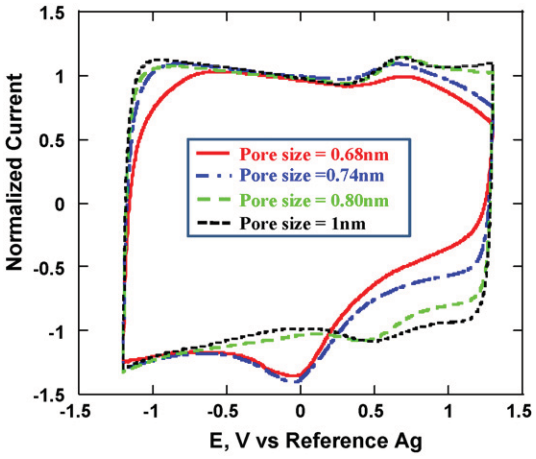

Fig. 4. Normalized CVs of CDC samples in AN + 2 M EMITFSI electrolyte between −1.2 and +1.3 V/Ref at a scan rate of 100 mV/s.

is close to 0.7 nm, again in good agreement with the result deduced from Fig. 3.

It can be deduced from these findings that the average effective ion size of the solvated EMI^+ ions in pores is somewhat lower than that of the $TFSI^-$ ions, in spite the size of the bare ions being almost the same. This, however, could be explained by the different affinities of the electrolyte ions for the solvent molecules and different solvation energies. Computer simulations show the peaks for EMI^+ at 1.77, 2.16 and 2.53 nm and for $TFSI^-$ at 2.24 and 2.74 nm in the radial distribution function. These numbers suggest the most probable solvation radii for the respective ions solvated in AN. Thus, while $TFSI^-$ ions have a larger solvation shell compared to EMI^+ ions, in agreement with the effective ions sizes estimated from CME experiments, both solvated ions are too big to be accommodated in CDC pores. This supports our previous findings that there is at least partial desolvation of electrolyte ions when they enter pores under an applied potential [19].

3.3. *Kinetics study of the $TFSI^-$ adsorption on CDCs*

However, and even more interesting, some additional current peaks can be observed in Fig. 4 at ~0.7 V/Ref on positive scan and ~−0.1 V/Ref on negative scan. These peaks are more pronounced for the two lower pore size samples at 0.68 and 0.74 nm at ~0 V/Ref, i.e. in a potential range including the OCV value where the charge storage mechanism changes from the cation adsorption to anion adsorption.

To try to understand the significance of these peaks a complete cyclic voltammetry study has been carried out with the 0.68 and 1 nm pore size samples, at scan rates ranging from 10 up to 1000 mV s^{-1}.

Fig. 5 shows CVs recorded in AN + 2 M EMITFSI electrolyte between 10 and 100 mV s^{-1} for the 1 nm pore size sample, in the whole potential range (−1.2 to +1.3 V/Ref). The intensity of the two peaks visible on the anodic positive scan – peak A – as well as on the cathodic negative one – peak B – changes with the scan rate. The inset in Fig. 5 shows the change of the logarithm of the peak current versus the logarithm of the scan rate B on the full potential scan range. The slope of the plots is 0.91 and 0.9 respectively for peak A and peak B. This value is close to 1, meaning that peaks A and B can be attributed to a capacitive charge storage mechanism not diffusion limited, according to (Eq. (2)):

$$I = Cd\,A\,\nu \tag{2}$$

where I is the current, Cd the capacitance (F m^{-2}), A the surface area (m^2) and ν the scan rate (V s^{-1}) [28].

Eq. (2) applies for the charge/discharge of the double layer capacitance or for fast redox surface reactions leading to a pseudocapacitive storage [29], where the electrode surface is accessible without any diffusion limitation. This surface process observed here is highly reversible as can be seen from the peak potentials and occurs in addition to the double layer charge/discharge capacitance.

Fig. 6 shows the CV for the 0.68 nm pore size sample recorded at 10 mV s^{-1} in AN + 2 M EMITFSI electrolyte. When the potential scan is limited between −1.2 and 0.5 V/Ref, the CV indicates a double layer capacitive behaviour. When the potential is scanned up to 1.3 V/Ref, the electrochemical signature is very different from that of the previous large pore size sample. On positive scan, a sharp current decrease is visible after a bump (A′) at potentials higher than 0.8 V/Ref. On the reverse potential scan, a huge cathodic peak B′ can be seen at about 0.2 V/Ref, before the current goes back to a constant value associated with the traditional double layer capacitive behaviour. The current decrease in the A′ zone and the cathodic peak B′ thus appears to be linked since peak B′ is not present when the potential scan is limited to +0.5 V/Ref. The change of the logarithm of the peak current versus the logarithm of the scan rate has been plotted for peak B′, in the 10–100 mV s^- potential scan rate range. Above 100 mV s^{-1}, the peak current cannot be distinguished from the double layer capacitive contribution.

The change of the maximum current peak with the potential scan rate for a reversible diffusion-controlled reaction is given by the Randles–Sevcik equation [30] (Eq. (3))

$$Ipeak = 0.4463\,(nF)^{3/2}\,A\,C\left(\frac{D}{RT}\right)^{1/2} \times \nu^{1/2} \tag{3}$$

where *Ipeak* is the maximum peak current, n the number of electrons involved, F the Faraday constant (A s), C the concentration of the diffusing species (mol cm^{-3}), D the diffusion coefficient of the diffusing species (cm^2 s^{-1}) and ν the potential scan rate (V s^{-1}). This equation applies to any charge transfer reaction under the diffusion control of the reactants to the electrode surface or the diffusion control of the products leaving the electrode surface. Accordingly, it can

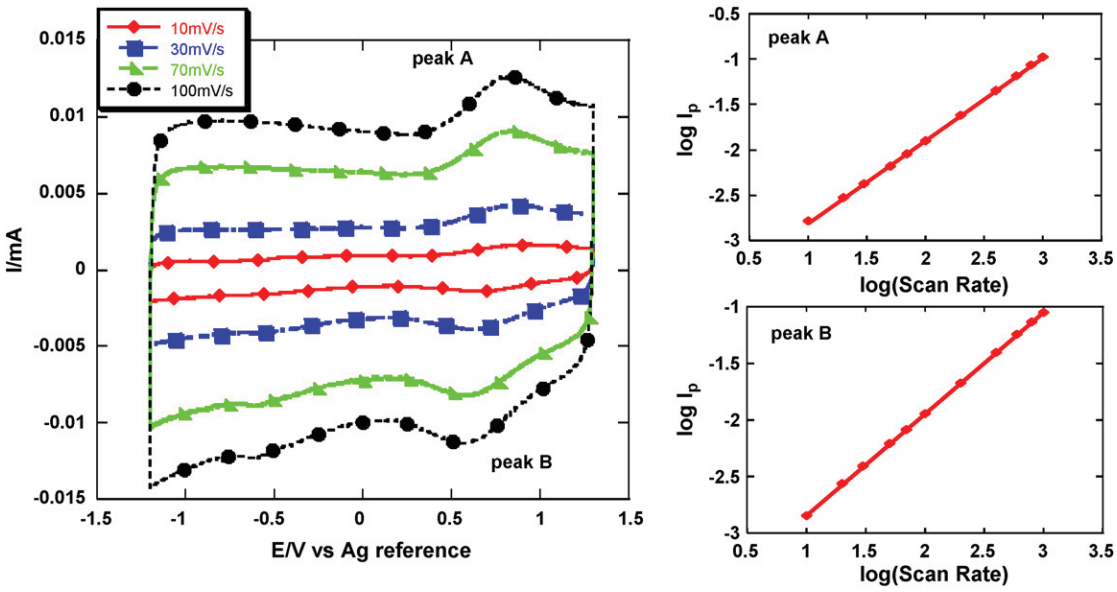

Fig. 5. CVs recorded at 10, 30, 70 and 100 mV s^{-1} for the 1 nm pore size sample, in AN + 2 M EMITFSI electrolyte. Inset: change of the logarithm of the peak current versus the logarithm of the potential scan rate, for peaks A and B.

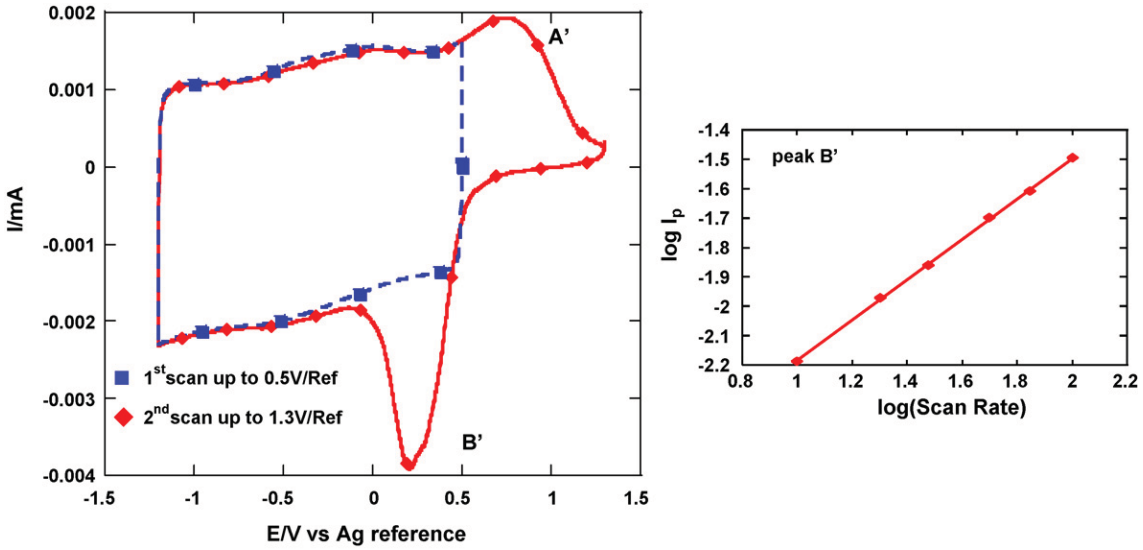

Fig. 6. CV for the 0.68 nm pore size sample recorded at 10 mV s^{-1} in AN + 2 M EMITFSI electrolyte, in the −1.2 up to 0.5 V/Ref potential range (1st scan) and the −1.2 up to 1.3 V/Ref potential range (2nd scan).

be used to describe a redox reaction as well as the ion transfer at an interface [30].

The slope of the log(*Ipeak*) versus log(ν) plot is 0.65 for the peak B′ (see inset in Fig. 6). This value is close to 0.5, meaning that the reaction observed with the 0.68 nm pore size sample seems to be under diffusion control. This small deviation from the theoretical 0.5 value can be explained by the nature of the electrode used in these experiments. By using porous carbon as the working electrode, we are not in the ideal case of a smooth, planar electrode used in Eq. (3) and the geometric dispersion due to the porous network may explain the difference observed.

Fig. 7 shows the influence of a potentiostatic holding at 1.3 V/Ref for the 0.68 nm pore size sample. A first CV was firstly done at 10 mV s^{-1} within the full potential range. Then, the scan was stopped at 1.3 V/Ref during the positive scan and the potential was kept at this value for 30 min; a second CV was further recorded within the full potential range. On Fig. 7, it can be seen that the B′ peak intensity increases after the potentiostatic holding at 1.3 V/Ref. There is thus a clear relationship between the current decrease observed in the A′ region and the cathodic peak B′.

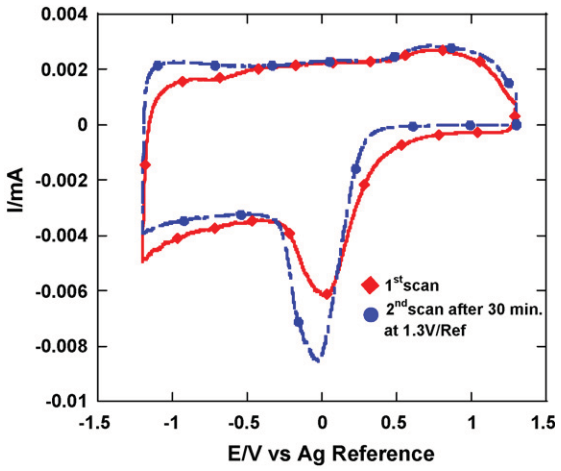

Fig. 7. CV for the 0.68 nm pore size sample recorded at 10 mV s^{-1} within the −1.2 up to 1.3 V/Ref potential range in AN + 2 M EMITFSI, before (squares) and after (circles) a 30 min potentiostatic holding at 1.3 V/Ref.

4. Discussion

Having a look to Figs. 5 and 6, it can be first stated that the large pore size (1 nm) and the small pore size samples show two different electrochemical signatures in the 0 V to 1.3 V/Ref potential range where the $TFSI^-$ anion adsorption occurs. For a carbon pore size slightly larger than the anion size, i.e. for the 1 nm pore size carbon, two reversible peaks appear at 0.7 V/Ref linked with a fast, surface storage process since no diffusion control appear within the 10–1000 mV s^{-1} potential scan range. Additionally, these peaks appear in addition to the double layer capacitance identified on the CV by the characteristic rectangular shape [29]. Both double layer capacitive and pseudo-capacitive storage can be described by Eq. (2). The latter should involve the presence of a reversible redox shuttle in the electrolyte or some redox surface functional groups on the carbon surface. However, once prepared, all the carbon samples studied here were annealed 1 h at 600 °C under H_2 atmosphere to reduce any potential surface functional group. Additionally, the CV of the same 1 nm pore size carbon sample in acetonitrile + 1.5 M $(C_2H_5)_4N^+,BF_4^-$ electrolyte does not show any reversible peak in the 0–1 V/Ref potential range [19], even up to 1.3 V/Ref (not shown). Accordingly, the solvent/carbon interface is not likely to be involved in a pseudo-capacitive storage mechanism linked with any reversible surface redox reaction that could have been due to the presence of any surface functional group or redox shuttle.

When the carbon pore size is decreased below the effective size of the anion (0.68 nm carbon sample), the current largely drops at potential higher than 0.7 V/Ref on the positive scan. Similar electrochemical behaviour has been previously reported [19,31] and assigned to a decrease in the pore accessibility for the ions. In the present case, the CV shows the limited accessibility of the $TFSI^-$ anions to the small 0.68 nm pores. On the reverse scan, the huge cathodic peak occurring at 0.3 V/Ref is mainly associated with a diffusion-controlled process. During this reverse scan, the $TFSI^-$ ions are forced by the electrostatic interaction to leave the carbon surface. Accordingly, we assume that this peak is linked with the removal of the $TFSI^-$ anions that were forced to enter the small pores during the positive scan. $TFSI^-$ ions have a high form factor so that ion removal from these narrow pores is hindered and rotation and alignment of ions in specific direction will be required to move them through the porous network and the diffusion of these

anions to exit the carbon pores controls the cathodic discharge process. Necks between the pores smaller than the average pore size might be present in the carbon structure and enhances this diffusion control. These CVs in Fig. 7 confirm this hypothesis, where the increase of the peak current B′ could be due to the increased number of $TFSI^-$ adsorbed during the potentiostatic holding at 1.3 V/Ref.

These results are consistent with recent data reported by Aurbach's group with microporous carbons in PC + 1 M $(C_2H_5)_4N^+,BF_4^-$ electrolyte [17]. They proposed a mechanism where desolvated $(C_2H_5)_4N^+$ cations could be partially trapped into small pores of comparable diameter after overcoming an activation barrier associated with the partial ion desolvation and the re-organization of the solvent molecules inside the pores. Once the barrier is overcome, the gain in free energy to accommodate the ions in these sites is positive thanks to the ion–carbon pore wall interaction [17], and the situation is compared with an ion in a potential well. Cation detrapping was observed by applying a high anodic overvoltage leading to the electrostatic repulsion between the pore walls and the cation. In the present work, the same mechanism is suspected to occur during the anion adsorption/desorption for the 0.68 nm pore size sample, except that the ion desorption can be achieved for a cathodic overvoltage of −0.55 V, which is the peak potential difference $\Delta Ep' = E_{peakB'} - E_{peakA'}$ between peaks B′ and A′ (Fig. 6).

When the carbon pore size is increased to 1 nm, i.e. when the pore size is in the same range or slightly larger than the effective ion size, $TFSI^-$ ions have access to the carbon pores, and hence the charge storage mechanism is not anymore controlled by the diffusion of the anions (see Fig. 5). The activation barrier to overcome is decreased as compared to the small pore size sample since $TFSI^-$ ions have now easier access to the pores. Ions stand in an energetically favourable configuration with specific interactions thanks to a closer distance from the carbon pore walls; this is associated with the appearance of peaks A and B on the CV (Fig. 5). The couple of peaks A and B are related to a highly reversible process since the peak potential difference $\Delta Ep = E_{peakB} - E_{peakA}$ is decreased down to −0.22 V as compared to $\Delta Ep'$ and is roughly constant within the 10–100 mV s^{-1} range (see Fig. 5) [28]. Peaks A and B define a potential for this reversible process, which is linked with an activation energy. In the specific configuration where the effective ion size is in the same range as the carbon pore size like for the 1 nm pore size sample, the peak A observed in charge (positive scan) could be linked with the activation energy barrier to overcome to partially desolvate the ions and re-organize the solvent molecules inside the pores, like suggested by Aurbach's group [17]. On the reverse scan, this process is reversible and an extra-capacitance is delivered which is about 25–30% of the total capacitance at 10 mV s^{-1}. It is one of the first time that such a reversible phenomenon is observed with double layer capacitance and it is difficult at this stage to propose some definitive answer to explain this reversible extra-capacitance. The re-organization of the solvent molecules in the pores or an increase of the electrostatic interactions between the ions and the carbon pore walls in this confined environment leading to an electrosorption- or a chemisorption-like sorption process could explain this extra-capacitance observed when the ion size is in the same range as the pore size. In this case, the associated reversible peaks A and B would be linked with the additional activation energy created by this process, differently from the case of a standard ion adsorption process in larger pores. Further work will be needed to get a better understanding of this reversible process, and a set of experiment has been launched in different electrolytes. Beyond that, from a fundamental point of view, there is a clear lack of understanding of the double layer charging in the confined space of micropores, where there is no room for the formation of the Helmholtz layer and diffuse layer expected at a solid–electrolyte interface. Computational modeling using Molecular Dynamics or ab initio methods would be for instance of great help in addressing the ion size in these sub-nanometer pores as well as the solvent reorganization, that are one of the keys to design the next generation of high energy density EDLCs.

5. Conclusions

The study of the EMI, TFSI ionic liquid as a model electrolyte in a non-associative environment in a 3-electrode configuration using microporous Ti-CDCs electrodes with a narrow distribution of micropores produced results that are in agreement with our previous study performed under a 2-electrode configuration and have affirmed that maximum capacitance can be achieved when the carbon pore size is in proximity of the ion size.

Extents of desolvation of the electrolyte ions upon adsorption into the pores under an applied potential were established. From the CVs recorded at 100 mV/s, the effective sizes of adsorbed ions are found to decrease in the order: $TFSI^-$ in AN > EMI^+ in AN > $EMI^+ \cong TFSI^-$. This confirms that although the bare sizes of the neat electrolyte ions (EMI^+ and $TFSI^-$) are fairly close, they have different affinities for the solvent molecules (AN), hence resulting in different extent of solvation and therefore different solvated ion sizes.

The electrochemical kinetics study of the small pore size CDC sample (0.68 nm) in AN + 2 M EMI^+, $TFSI^-$ electrolyte showed that the $TFSI^-$ anion adsorption in the pores was a diffusion-controlled process because of the lack of accessibility due to size effect. When the carbon pore size was increase to be close the ion size, for the 1 nm CDC sample, a set of highly reversible peaks appear on the capacitive CV leading to 25% extra-capacitance at 10 mV s^{-1} scan rate. This reversible extra-capacitance is suspected to be issued from an increase of the electrostatic interactions between the ions and the carbon pore walls in this confined environment. Further work is needed to fully characterize the ion transport and adsorption in these sub-nanopores, but these new results confirm that matching the pore size of carbon to the ion size of electrolyte is of vital importance for optimizing specific capacitance, when using either solvated or solvent-free ionic liquid electrolytes.

Acknowledgements

We are grateful to Mr. Carlos Perez (Drexel University) for calculating the solvated ion size. J. Chmiola was supported by an NSF GRFP Fellowship. Y. Gogotsi was partially funded through the Pennsylvania Nanotechnology Institute (NTI) and PA Nano grants to Y-Carbon, Inc. C. Largeot and J. Ségalini were supported by Délégation Générale pour l'Armement. R. Lin and P. Huang were funded through the European Erasmus Mundus programme from the European Commission.

References

[1] P. Simon, Y. Gogotsi, Nature Materials 7 (2008) 845.
[2] J.R. Miller, P. Simon, Science 321 (2008) 651.
[3] J. Gamby, P.L. Taberna, P. Simon, J.F. Fauvarque, M. Chesneau, Journal of Power Sources 101 (2001) 109.
[4] G. Salitra, A. Soffer, L. Eliad, Y. Cohen, D. Aurback, Journal of the Electrochemical Society 147 (2000) 2486.
[5] C. Vix-Guterl, E. Frackowiak, K. Jurewicz, M. Friebe, J. Parmentier, F. Beguin, Carbon 43 (2005) 1293.
[6] L. Eliad, G. Salitra, A. Soffer, D. Aurbach, Langmuir 21 (2005) 3198.
[7] L. Eliad, E. Pollak, N. Levy, G. Salitra, A. Soffer, D. Aurbach, Applied Physics A-Materials Science & Processing 82 (2006) 607.
[8] J. Dzubiella, J.P. Hansen, Journal of Chemical Physics 122 (2005) 23706.
[9] J.M. DiLeo, J. Maranon, Journal of Molecular Structure: THEOCHEM 729 (2004) 53.
[10] M. Carrillo-Tripp, H. Saint-Martin, I. Ortega-Blake, Physical Review Letters 93 (2004) 168104.
[11] E. Lust, A. Jänes, M. Arulepp, Journal of Solid State Electrochemistry 8 (2004) 488.
[12] J. Leis, M. Arulepp, A. Kuura, M. Latt, E. Lust, Carbon 400 (2006) 2122.

[13] J. Chmiola, G. Yushin, Y. Gogotsi, C. Portet, P. Simon, P.-L. Taberna, Science 313 (2006) 1760.
[14] J. Chmiola, C. Largeot, P.L. Taberna, P. Simon, Y. Gogotsi, Angewandte Chemie-International Edition 47 (2008) 3392.
[15] J.S. Huang, B.G. Sumpter, V. Meunier, Angewandte Chemie-International Edition 47 (2008) 520.
[16] J.S. Huang, B.G. Sumpter, V. Meunier, Chemistry-A European Journal 14 (2008) 6614.
[17] D. Aurbach, M.D. Levi, G. Salitra, N. Levy, E. Pollak, J. Muthu, Journal of The Electrochemical Society 155 (2008) A745.
[18] C. Largeot, C. Portet, J. Chmiola, P.-L. Taberna, Y. Gogotsi, P. Simon, Journal of the American Chemical Society 130 (2008) 2730.
[19] R. Lin, P.L. Taberna, J. Chmiola, D. Guay, Y. Gogotsi, P. Simon, Journal of the Electrochemical Society 156 (2009) A7.
[20] P.I. Ravikovitch, A. Neimark, Colloids and Surfaces A 187–188 (2001) 11.
[21] R. Dash, J. Chmiola, G. Yushin, Y. Gogotsi, G. Laudisio, J. Singer, J. Fischer, S. Kucheyev, Carbon 44 (2006) 2489.
[22] C. Portet, P.L. Taberna, P. Simon, C. Laberty-Robert, Electrochimica Acta 49 (2004) 905.
[23] C. Portet, P.L. Taberna, P. Simon, E. Flahaut, C. Laberty-Robert, Electrochimica Acta 50 (2005) 4174.
[24] C. Cachet-Vivier, V. Vivier, C.S. Cha, J.Y. Nedelec, L.T. Yu, Electrochimica Acta 47 (2001) 181.
[25] M. Zuleta, P. Bjornbom, A. Lundblad, G. Nurk, H. Kasuk, E. Lust, Journal of Electroanalytical Chemistry 586 (2006) 247.
[26] C. Portet, J. Chmiola, Y. Gogotsi, S. Park, K. Lian, Electrochimica Acta 53 (2008) 7675.
[27] J. Huang, B.G. Sumpter, V. Meunier, Angewandte Chemie 46 (2007) 1.
[28] A.J. Bard, L.R. Faulkner, Electrochemical methods, fundamentals and applications, Wiley editor, 2nd edition, 2001.
[29] B.E. Conway, Electrochemical Supercapacitors: Scientific Fundamentals and Technological Applications, Kluwer, 1999.
[30] H. Girault, Analytical and Physical Chemistry, EPFL editors, ISBN: 2-940222-03-7.
[31] R. Mysyk, E. Raymundo-Pinero, F. Beguin, Electrochemistry Communications 11 (2009) 554.